J. Mol. Biol. (1979) **131**, 137–155

Crystal Structure of Demetallized Concanavalin A: the Metal-binding Region

MENAHEM SHOHAM, ADA YONATH, JOEL L. SUSSMAN, JOHN MOULT
WOLFIE TRAUB AND A. JOSEPH KALB (GILBOA)

Departments of Structural Chemistry, Chemical Physics and Biophysics
The Weizmann Institute of Science, Rehovot, Israel

(Received 26 June 1978, and in revised form 9 February 1979)

We have determined the crystal structure of demetallized concanavalin A, at a resolution of 3·2 Å, by molecular replacement using the known structure of native concanavalin A. Refinement of the initial model using a constraint-restraint reciprocal-space least-squares procedure caused the conventional crystallographic agreement (R) factor to decrease from 0·47 to a final value of 0·26. There are significant conformational changes in the metal-binding region involving residues Asp19 and His24, which are substantially closer to each other than in native concanavalin A. These residues form an internal salt bridge which does not exist when the metal ions are attached to the protein. The binding site for transition-metal ions is still intact, but the calcium site is not, since one of its two carboxylic ligands, Asp19, is unavailable. Flexibility is observed for one of the transition-metal ligands, Glu8, as well as for some segments of the backbone. The latter could account for the increased susceptibility of demetallized concanavalin A to proteolysis.

1. Introduction

Concanavalin A is a saccharide-binding protein of the Jack bean (Sumner, 1919). Its saccharide-binding properties in solution have been shown to depend on the presence of two metal ions in the protein (Sumner & Howell, 1936; Yariv *et al.*, 1968). One of these is bound at a site (S1) with specificity for divalent metal ions having affinity for nitrogen ligands (e.g. Mn^{2+}, Co^{2+}, Zn^{2+}). Occupation of S1 by a metal ion is attended by the formation of a second metal-binding site (S2) with high specificity for Ca^{2+} (Kalb & Levitzki, 1968; Shoham *et al.*, 1973).

Spectroscopic studies of concanavalin A–metal complexes indicate that binding of the Ca^{2+} ion at S2 leads to a rather rigid organization of the transition metal-binding site, S1 (Nicolau *et al.*, 1969; Meirovitch & Kalb, 1973; Barber & Carver, 1973; Kalb & Pecht, 1973; Meirovitch *et al.*, 1974; Goldammer & Zorn, 1974). Enzymic digestibility is found to decrease greatly on occupation of S1; the native form, with both S1 and S2 occupied, is virtually impregnable to proteolytic enzymes (Blumberg & Tal, 1976).

The details of the structural changes in the protein on successive occupation of the two metal-binding sites can be elucidated by comparisons among X-ray structures of metal-free concanavalin A, its transition metal complex, and the native protein containing both metals. Of these, the native form has been crystallized and its X-ray structure has been described in some detail (Edelman *et al.*, 1972; Hardman & Ainsworth, 1972; Becker *et al.*, 1975).

0022-2836/79/180137-19 $02.00/0

In the present study, we have determined the structure of demetallized concanavalin A. The crystals, which have been described elsewhere (Jack *et al.*, 1971), have the space group $P2_122_1$ with axial lengths $a = 84{\cdot}3$ Å, $b = 91{\cdot}2$ Å, $c = 61{\cdot}1$ Å and are related to crystals of the native form, with space group $I222$, by a small rotation of the structure about the crystallographic y-axis. These crystals are well suited to such a comparative study because they can be converted, in the solid state, to crystals of the native form ($I222$) simply by soaking them for several days in a dilute solution of Mn^{2+} and Ca^{2+}.

The unit-cell dimensions and protein content are nearly identical in the two crystal forms. However, in the native crystal the asymmetric unit is a single polypeptide subunit of M_r 26,000 whereas in the demetallized crystal it is a dimer of M_r 52,000. The similarity between these crystals prompted us to use the molecular-replacement method (Rossmann, 1972) for the structure determination.

X-ray studies of native concanavalin A have identified the amino acid side-chains which participate in the two metal-binding sites. The amino acids involved are included in the sequence of residues 7 to 35 from the N-terminus. In this study, we have focused our attention on this region, shown schematically in Figure 1. The differences which we find between the native and demetallized proteins form the structural basis for a mechanistic model of the interactions in solution between the two metal-binding sites, which we have reported briefly elsewhere (Shoham *et al.*, 1978).

2. Experimental

(a) *Data collection and processing*

Demetallized concanavalin A was prepared and crystallized as previously described (Kalb & Levitzki, 1968; Jack *et al.*, 1971). These crystals diffract out to a minimum spacing of about 3 Å.

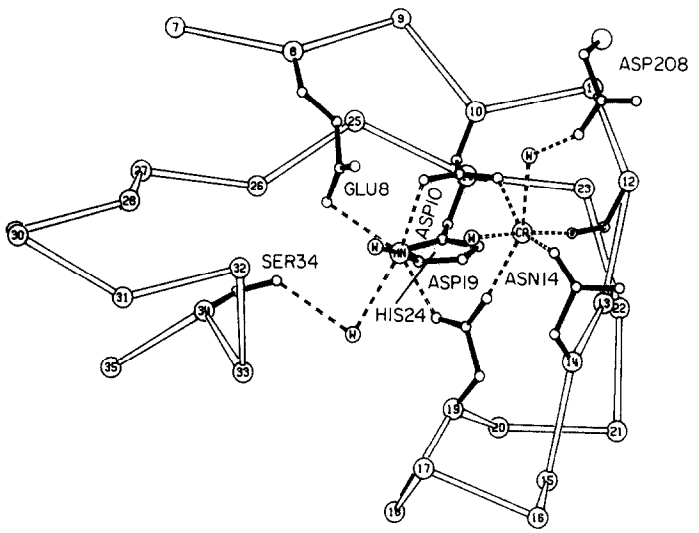

FIG. 1. Schematic view of the Mn^{2+} and Ca^{2+} binding region in native concanavalin A (based on co-ordinates kindly supplied by Dr K. Hardman). The open lines represent virtual bonds between successive alpha-carbon atoms of residues 7 to 35. The side-chain ligands are shown in solid lines, and the co-ordination of the metal ions in dashed lines. Water molecules are designated "W". Note that all the direct protein ligands are within the loop of residues 8 to 24.

Intensity measurements were made on a Nonius CAD-3 automatic diffractometer, fitted with a 40-cm helium-filled tube between crystal and counter, and using Ni-filtered CuKα radiation. Measurements were made with an ω-scan technique (Watson *et al.*, 1970). The scan width was chosen wide enough to cover at least 1·5 times a complete profile of each reflection, and the positions of the reflections were determined by maximizing the integrated intensities over 0·66 of the scan width. Twice the integrated intensity over the remaining points was subtracted as background.

An empirical absorption correction was applied as described by North *et al.* (1968). Absorption measurements were made several times during the course of data collection and, as no significant changes were observed in absorption curves for the same crystal, these were averaged. Radiation damage and crystal misalignment were monitored by remeasuring 8 standard reflections after every 100 intensity measurements. An empirical correction for radiation damage, based on the decay in the monitor reflections, was applied up to a maximum intensity loss of 15%, after which the crystal was discarded.

Data were collected from 3 crystals in overlapping radial shells. No significant intensities were observed beyond 3·2 Å. Data from the different crystals were scaled and merged using common reflections (Rollett & Sparks, 1960). The average deviation from the mean ($\Sigma| |F| - |\bar{F}| |/\Sigma|\bar{F}|$) was 0·052 for about 1000 structure amplitudes common to crystals 1 and 2 and 0·076 for about 500 common to crystals 2 and 3.

A chloroplatinate derivative of demetallized concanavalin A was prepared by soaking crystals of the protein in a crystallizing medium containing 0·1 mM-K_2PtCl_4 for 7 days. All 3 centric projections of parent and derivative crystals were recorded on 14° precession photographs at 100 mm specimen-to-film distance with Ni-filtered CuKα radiation, and intensities measured on an Optronics P-1000 microdensitometer. Structure amplitudes were derived with a program kindly supplied by Dr Gerson Cohen.

(b) *Orientation and translation search*

The change in the crystallographic space group from $I222$ in native concanavalin A to $P2_122_1$ in the demetallized form can be accounted for by a rotation of a rigid tetrameric cluster of protomer subunits about the 2-fold axis along y (Jack *et al.*, 1971). Thus, the dyads along the x- and z-axes in the native form become non-crystallographic in demetallized concanavalin A, which has an asymmetric unit composed of two protomers related by a local dyad. Translation of the intact tetramer along the y-axis is also consistent with the change in space group, but translation along or rotation about the x- and z-axes would imply relative movements of dimers within the tetramer.

We have investigated all these possible motions using, as a search model, a rigid dimer of subunits I and II which, because of their many intermolecular contacts, are believed to constitute the stable dimer in solution (Reeke *et al.*, 1975). Atomic co-ordinates for the search model were kindly supplied by Dr Karl Hardman (Hardman & Ainsworth, 1975); the metal ions were not included. The orientation and translation search was based on computation of conventional crystallographic agreement (R) factors between observed structure amplitudes and those calculated for the search model in the various possible positions. Investigations were first made of movements of the intact tetramer by rotation about the y-axis or translation along it. Subsequently, after the best position was found for the tetramer (7° rotation about the y-axis, see Results), further possible movements of the dimer were investigated in terms of translations along the other 2 axes or combinations of rotations about them.

(c) *Map interpretation and structure refinement*

A portion of an initial electron density map is shown in Fig. 2. The coefficients here are $(2|F_o| - |F_c|)\exp(i\alpha_c)$, where $|F_c|$ and α_c are the amplitude and phase of the native structure, rotated 7° in this cell, and $|F_o|$ are the observed structure factor amplitudes for the demetallized structure. The unweighted R factor between these $|F_o|$ and $|F_c|$ is 0·47 for data to 3·2 Å resolution. As might be expected for such a starting model, inspection of the map shows that following chain continuity is difficult and detailed interpretation would be unreliable. To overcome this difficulty we have refined the structure away from the starting model and experimented with the usefulness of different types of maps.

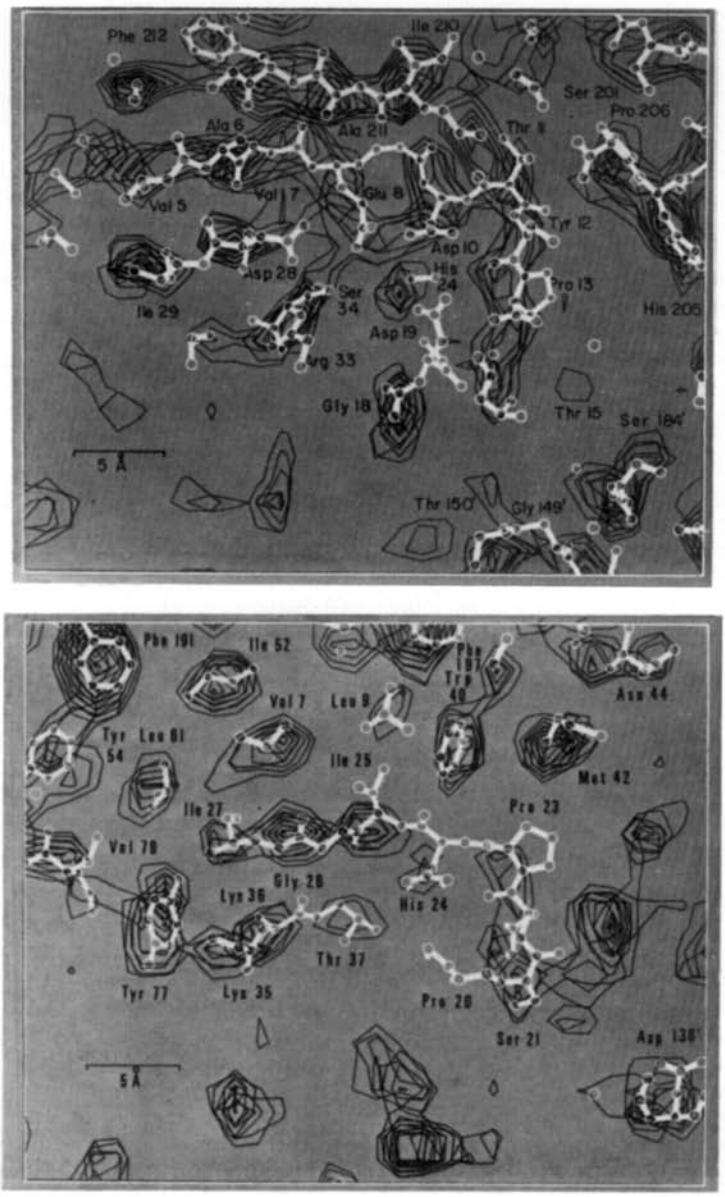

FIG. 2. Two successive 5 Å-thick portions of the electron density map of demetallized concanavalin A in the metal-binding region *prior to refinement*. The coefficients of the Fourier summation are $(2|F_o| - |F_c|)\exp(i\alpha_c)$. Contours are drawn from a level corresponding to the standard deviation (σ) of the electron density map in equal intervals of half that value.

$$\sigma = \left(\sum_{i=1}^{n} \rho_i^2/n\right)^{1/2},$$

where ρ_i is the electron density at each of the n grid points in the non-protein portion of the map (more than 1·5 Å from any protein atom). Superimposed is the initial atomic model. Note the lack of chain continuity at residues 23 to 25 and the high level of unmatched density in some parts of the non-protein region.

A constrained-restrained reciprocal-space least-squares refinement method (CORELS) was used. This method was developed for the refinement of the transfer RNA structure at a similar resolution (Sussman *et al.*, 1977), and has now been adapted for protein work (O. Herzberg and J. L. Sussman, manuscript in preparation). In this procedure each amino acid residue is considered to be an independent unit of the structure, but is restrained to have a suitable spatial relationship to neighbouring residues in the chain. Within each unit, dihedral and main-chain bond angles, as well as the composite temperature factors of groups of atoms, may be refined. All restraints are implemented by means of flexible "springs" between pairs of atoms, and by suitably varying the "stiffness" of these springs it is possible to make the distances between pairs of atoms as close to standard lengths as is desired.

The strategy we used in refining the structure (that is, minimizing the differences between the observed and calculated structure factors) was initially to vary only a minimal number of parameters and gradually to allow more to vary in the following order.

(1) Rigid-body movements (rotation and translation) of individual amino acids, with restraints between adjacent residues in the sequence to maintain proper inter-residue geometry.

(2) Variation of the side-chain dihedral angles.

(3) Introduction of "repulsive" springs between non-bonded atoms to minimize total repulsive interaction due to bad van der Waals' contacts.

(4) Refinement of 2 group temperature factors per residue, 1 for main-chain atoms (N, C_α, C , C′, O) and one for the remaining atoms.

This sequence was designed to allow the biggest movements of large groups of atoms to occur first. The asymmetric unit refined consists of the 3612 non-hydrogen and non-metal atoms of the dimer, and the behaviour of equivalent residues in the 2 monomers provided a check of the accuracy of the results.

The usefulness of 3 different maps was investigated. These were:

(1) "Chopped" difference maps, with coefficients $(|F_o| - |F_c|)\exp(i\alpha_c)$. The calculated structure factor amplitudes and phases excluded contributions from the part of the structure under investigation. These maps have the advantage that no model information is included for the part of the structure under study and so an unbiased interpretation may be made.

(2) A difference map, with coefficients $(|F_o| - |F_c|)\exp(i\alpha_c)$. This map will have no features where the model is correct, negative features where atoms have been incorrectly placed, and positive features where they have been omitted from the model. Although difficult to interpret in detail at this resolution, this type of map has the advantage of highlighting incorrectly placed features or disorder. Fig. 3 shows part of such a map where a group of atoms have been misplaced in the demetallized structure. Comparison of this with the relatively clean final difference maps demonstrates the usefulness of the map in this regard. Analysis of the average density around individual atomic positions in such maps allows improvement or deterioration in the model during the refinement process to be followed semiquantitatively.

(3) A map with coefficients $(2|F_o| - |F_c|)\exp(i\alpha_c)$, which may be written as $F_c\exp(i\alpha_c) + 2(|F_o| - |F_c|)\exp(i\alpha_c)$, where the 1st term represents an exact calculated map of the current model and the 2nd a map of the difference density between this model and the correct structure; the factor 2 in this term partly compensates for the approximation involved (Luzzati, 1953). Thus the sum of these 2 terms gives approximately the electron density of the correct structure.

3. Results

(a) *Orientation and translation search*

Figure 4 shows the behaviour of the standard R factor as a function of the rotation of the dimeric asymmetric unit about the y-axis. Based on these results, the rotation

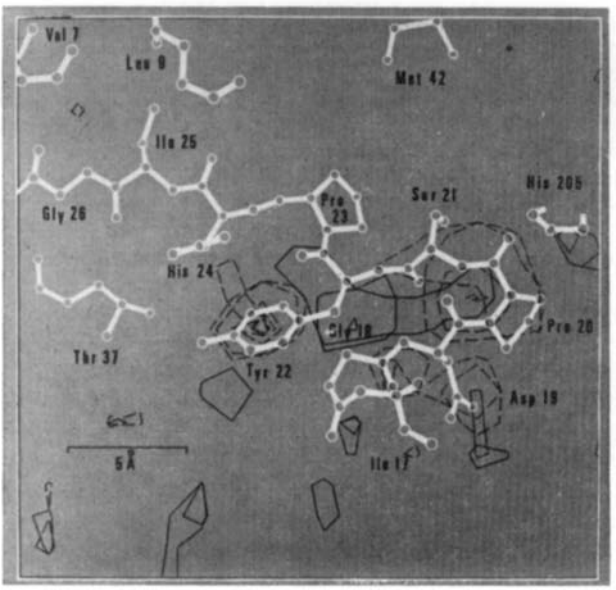

FIG. 3. A 5 Å-thick portion of a difference electron density map of a part of protomer I, based on a model in which residues 18 to 22 are misplaced. The coefficients of the Fourier summation are $(|F_o| - |F_c|)\exp(i\alpha_c)$. Positive and negative contours are shown in solid and dashed lines, respectively, at equal intervals of twice the standard deviation (σ) of the non-protein region of the map. This map shows how easy it is to detect incorrect features in the model, and may be compared with the much cleaner difference map for the final refined model, shown in Fig. 7.

angle was taken to be $7{\cdot}0° \pm 0{\cdot}1°$. A systematic investigation of all possible combinations of rotations about the x- and z-axes, in 5° intervals (after 7° rotation about the y-axis), showed only R factors greater than 50% for 83 strong reflections (cf. Fig. 4(a)) except near zero rotations about both axes. A further search in 1° intervals indicated that the minimum R value corresponds, in fact, to 0°, 7°, and 0° rotations about the x, y and z-axes, respectively.

A similar search involving translations along x, y and z independently for distances of up to 6 Å gave the lowest R factor for translations of $0{\cdot}0 \pm 0{\cdot}2$ Å in all directions. Shifts as small as 0·5 Å yield an R factor 1% higher than for the zero shifts.

These results are supported by the heavy-atom co-ordinates which we found for the tetrachloroplatinate derivative of demetallized concanavalin A. The two sites, which were determined from Patterson projection maps, have co-ordinates (0·00, 0·06, 0·06) and (0·00, −0·06, 0·06) to an accuracy of 0·01 of the axial lengths. These co-ordinates are indistinguishable from the heavy-atom positions of this derivative of native concanavalin A (Weinzierl & Kalb, 1971; Hardman *et al.*, 1971; Quiocho *et al.*, 1971) and indicate that any translation must be less than the maximum error in the co-ordinates (about 1·5 Å). These heavy-atom co-ordinates are, however, not sensitive to small rotations, and the 7° rotation about the y-axis (located at $x = 0$, $z = 0$) causes these positions to shift by only 0·4 Å.

(b) *Refinement*

Tables 1 and 2 and Figures 5 and 6 summarize the refinement steps. As we let more parameters vary, such that the ratio of observations to parameters decreased from 2·4 to 1·9, the refinement remained reasonably well over-determined because of the

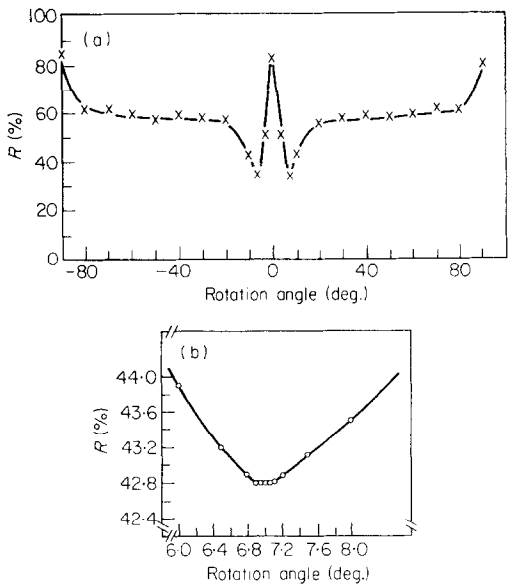

FIG. 4. Rotation search for a rigid dimer of native concanavalin A in the crystal lattice of demetallized concanavalin A. The ordinate is the agreement factor ($R = \Sigma||F_o| - |F_c||/\Sigma|F_o|$), where F_o and F_c represent the observed and calculated structure factors. The abscissa is the rotation angle about the y-axis. At rotations of 0° and $\pm 90°$ the space group is actually $I222$ rather than $P2_122_1$, which causes half the reflections to vanish. Therefore, the sum of discrepancies between F_o and F_c is highest at these angles. The curve is symmetrical with respect to the sign of the rotation angle, since for any particular orientation there will be 2 dimers (constituting a tetramer) rotated clockwise and, because of the space group, another 2 equivalent dimers rotated counterclockwise. (a) For a sample of 83 strong reflections. (b) A close-up in the vicinity of 7·0° rotation, computed from data for 5300 reflections with a minimum spacing of 3·2 Å.

approximately 6000 distance restraints. It should also be noted that when non-bonded restraints were introduced in step 10, the R factor did not increase. The average change in phases was 45° (r.m.s. 60°), which is about the same as has been found in other protein refinements (Watenpaugh *et al.*, 1973). A typical cycle, for one of the two monomers, using 7800 reflections, varying 2000 parameters simultaneously, with 1800 atoms and 6000 distance restraints, took 100 minutes and 1000 Kbytes on an IBM 370/168 computer. In retrospect, we realize that the refinement could have proceeded through fewer steps, but in part we were learning how to use the method. The R factor decreased from 0·47 for the unrefined model to 0·26 at the end of refinement. These values are for all 7800 reflections between 10 Å and 3·2 Å.

(c) *Electron density maps*

Part of the difference map calculated for the final structure is shown in Figure 7. The paucity of features is typical of the whole map and is in sharp contrast to Figure 3, which shows a difference map for part of the same region of the unit cell with several incorrectly placed residues. The electron density and refined structure for the entire metal-binding regions of protomers I and II are shown in Figure 8.

The interpretability of both $(2|F_o| - |F_c|)\exp(i\alpha_c)$ maps and "chopped" difference maps improved dramatically during the refinement. This can be seen by comparing

TABLE 1

Summary of refinement steps

Cycle	Refinement operation	R(%)	No. of reflections	No. of restraints	No. of variables	Comments
0	Generate starting co-ordinates by molecular replacement from native concanavalin A	42·8	5302	—	—	Data 10 Å to 3·2 Å medium and strong reflections
1	Rigid-body motion of individual amino acids, linked by inter-residue restraints	33·7	5302	3394	3318	Side-chain dihedral angles kept constant
2	Rigid-body motion of individual amino acids, linked by inter-residue restraints	30·2	5302	3394	3318	Side-chain dihedral angles kept constant
3	Rigid-body motion of individual amino acids, linked by inter-residue restraints	28·7	5302	3394	3318	Side-chain dihedral angles kept constant
4	Rigid-body motion of individual amino acids, linked by inter-residue restraints	33·5	7801	3394	3318	All data 10 Å to 3·2 Å side-chain dihedral angles kept constant
5	Rigid-body motion of individual amino acids, linked by inter-residue restraints	32·4	7801	3394	3318	All data 10 Å to 3·2 Å side-chain dihedral angles kept constant
6	Rigid-body motion of individual amino acids, linked by inter-residue restraints	31·8	7801	3394	3318	All data 10 Å to 3·2 Å side-chain dihedral angles kept constant
7	Rigid-body motion of individual amino acids, linked by inter-residue restraints	30·4	7801	3394	3950	Side-chain dihedral angles X_1 and X_2 allowed to vary, except for prolines
8	Rigid-body motion of individual amino acids, linked by inter-residue restraints	29·3	7801	3394	3950	Side-chain dihedral angles X_1 and X_2 allowed to vary, except for prolines
9	Rigid-body motion of individual amino acids, linked by inter-residue restraints	29·0	7801	3394	4050	Side-chain dihedral angles X_1 to X_4 allowed to vary, except for prolines

10	Rigid-body motion of individual amino acids, linked by inter-residue restraints	28·9	7801	6158	4050	Side-chain dihedral angles X_1 to X_4 allowed to vary, except for prolines. Additional restraints added to minimize repulsive interactions from bad contacts between non-bonded atoms
11	Rigid-body motion of individual amino acids, linked by inter-residue restraints	28·2	7801	6028	4050	The number of restraints was slightly reduced after refinement caused some non-bonded atoms to move further apart than a fixed minimum distance
12	Rigid-body motion of individual amino acids, linked by inter-residue restraints	27·9	7801	5993	4050	The number of restraints was slightly reduced after refinement caused some non-bonded atoms to move further apart than a fixed minimum distance
13	Rigid-body motion of individual amino acids, linked by inter-residue restraints	27·6	7801	5993	4050	Final cycle of refinement. Structure factors from this cycle are used for computation of final electron density maps
14	Group temperature-factor refinement: two per residue, one for the backbone atoms (N, C_α, C_β, C′ and O), and the other for side-chain atoms. (For Gly, Ala and Pro there is only one temperature factor.) All the rest of the parameters are kept constant	25·6	7801	0	856	This cycle was computed only for the purpose of establishing the relative flexibility of various groups in the protein and was not used in calculating electron density maps

TABLE 2

Some overall properties of the refined structure

R initial	= 0·470
R final	= 0·276
R group temp. factors	= 0·256
Estimate of error in final co-ordinates	= 0·6 Å†

		Mean	r.m.s.	Maximum	
Deviations of corresponding co-ordinates from the initial model (native concanavalin A)‡	Whole structure	1·0 Å	1·1 Å	5·0 Å	(terminal N of Arg172, protomer I)
	Backbone	0·9 Å	1·0 Å	2·4 Å	(C_α of Gly98, protomer I)
	Side-chains	1·2 Å	1·4 Å	5·0 Å	
Deviations of corresponding co-ordinates between protomer I and protomer II§		1·0 Å	1·2 Å	4·5 Å	(C_γ of Val75)
Deviations of phase angles from those of the initial model		45°	65°	180°	
Deviations from planarity of the peptide bond		4°	6°	31°	(Phe213–Ile214, protomer I)
Deviations of bond angles in the peptide plane from standard values¶	Angle (C_α-C-N)	3°	4°	11°	(Asn131–Gln132, protomer I)
	Angle (C-N-C_α)	6°	8°	27°	(Ser160–Ser161, protomer I)
	Angle (O-C-N)	3°	3°	11°	(Val79–Asp80, protomer II)
Deviations of the peptide bond length from a standard value¶		< 0·01 Å	0·01 Å	0·04 Å	

† Estimated from a comparison of co-ordinates between the two independently refined protomers. For this comparison some 500 backbone atoms N, C_α and C were used. The metal-binding region (res 7–35) as well as the regions of high flexibility in an external loop (res 115–124) and the carboxy-terminal part (res 235–237) were excluded for the purpose of this calculation.

‡ Co-ordinates of native concanavalin A from Hardman & Ainsworth (1975).

§ With the aid of a computer program to superimpose co-ordinates of protomer II onto those of protomer I in such a way as to minimize their corresponding deviations (Nyburg, 1974). All atoms included in calculation.

¶ The only bond length altered in the refinement process is the peptide linkage between successive residues, and the only bond angles varied are within the peptide plane. Standard bond lengths and bond angles according to Diamond (1974).

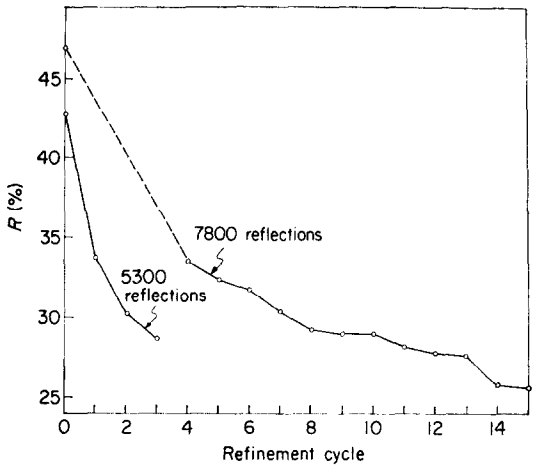

FIG. 5. Decrease of $R = \Sigma||F_o| - |F_c||/\Sigma|F_o|$ during the reciprocal-space refinement of demetallized concanavalin A. In the first 3 cycles a partial data set of 5300 reflections was used. From cycle no.4 the entire data set of 7800 reflections was used. The initial R factor for the full data set was 0·47 as indicated by the dashed line. For details of each refinement cycle see Table 1.

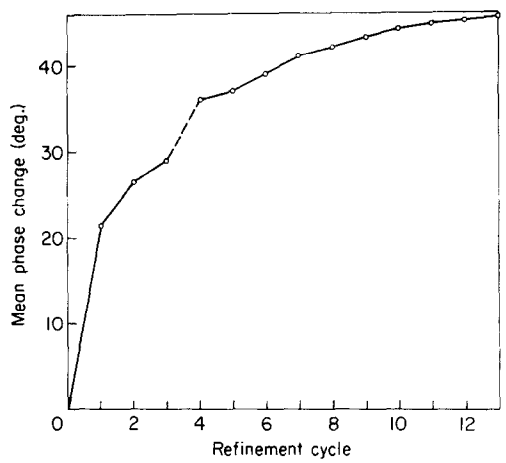

FIG. 6. Mean phase change of the calculated structure factors from those of the starting model, during the reciprocal-space refinement of demetallized concanavalin A. The dashed line indicates the incorporation of the entire data set.

Figure 2 with Figure 8(a) (middle and bottom) which show the same portion of map before and after refinement. In general, both types of map are very similar, but occasionally the chopped difference map lacks density where there is density in the other map and the difference map is relatively clean. Therefore, $(2|F_o| - |F_c|)\exp(i\alpha_c)$ maps were usually used for interpretation.

In general, the polypeptide chain can be traced reasonably well, but occasionally there is lack of density, for example at Pro20 in protomer I, and between residues 14 and 17 and at Arg33 in protomer II. Since in the difference map these features appear in troughs with no unmatched peaks nearby, we believe that they represent flexible segments of the structure. On the other hand, there are some unaccounted for extra peaks, both in the $(2|F_o| - |F_c|)\exp(i\alpha_c)$ map and in the $(|F_o| - |F_c|)\exp(i\alpha_c)$ difference map. Most of these are clearly outside the protein region, but a

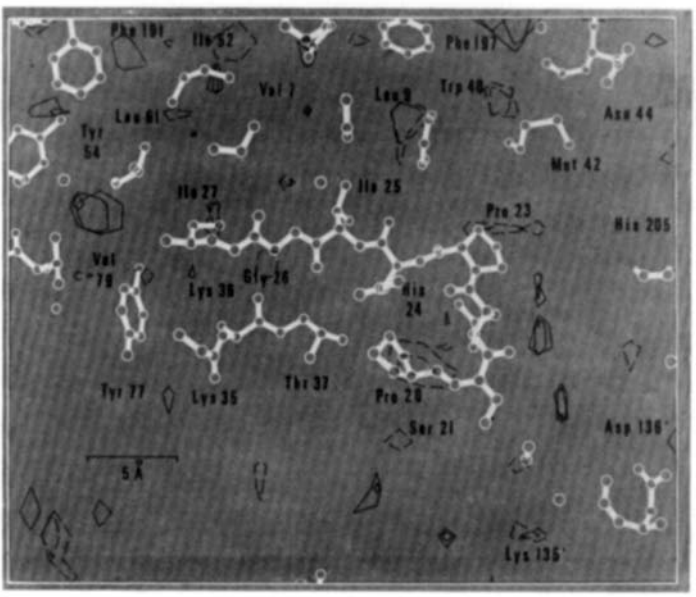

FIG. 7. A 5 Å-thick portion of the difference electron density map for the refined structure of demetallized concanavalin A in the metal-binding region of protomer I, sectioned along the z-axis. The coefficients of the Fourier summation are $(|F_o| - |F_c|) \exp(i\alpha_c)$. Positive and negative contours are shown in solid and dashed lines, respectively, at equal intervals of twice the standard deviation (σ) of the non-protein region of the map. Superimposed is the atomic model. Residue numbers designated with a superscript are from a neighbouring molecule.

possible exception is the peak situated near Ser21 (see Figs 7, 8(a) bottom, and 8(b) bottom). At an intermediate stage of the interpretation process, we tried to account for this density by an extended loop of residues 18 to 22. The difference map shown in Figure 3 clearly indicates this preliminary interpretation to be incorrect. We therefore believe this and the other extra peaks may represent ions or ordered solvent.

The group temperature-factor refinement provides a cross check on weak density features. The temperature factors, in fact, proved to be very sensitive to any lack of correspondence between atomic positions and electron density. Sometimes high temperature factors indicated only minor imperfections such as the ends of the side-chains of Ile4 (Fig. 8(b), top) or Ile29 (Fig. 8(a), middle) lying just on the edge of electron density. In other cases however they indicated what are evidently flexible segments in the structure which fall in troughs in the difference maps. As might be expected, most of the unusually high temperature factors were found to correspond to structural features on the surface of the molecule. Particularly high temperature factors were found for residues 118 to 122 in an external loop which is often found to be cleaved in the native structure (Edelman *et al.*, 1972) and for the carboxy-terminal residues 235 to 237.

(d) *The structure of the metal-binding region, residues 7 to 35*

The folding of the backbone in both protomers is very similar to that in native concanavalin A, but there is a slight, yet consistent, closing up around the "metal positions" (see Fig. 9). The more striking conformational differences are confined to Asp19 and His24, which are located closer to each other than in the native form. The

distance between the carbon atom of the Asp19 carboxyl group and either of the two nitrogen atoms of the imidazole ring of His24 diminishes by about 1 Å in both protomers. This is due to changes in the positions of both Asp19 and His24. However, the position of Asp19 is different in the two protomers. In protomer I, Asp19 is pointing away from the calcium position, thus increasing the Ca–C_γ (Asp19) distance from 3·5 Å to 5·5 Å, whereas in protomer II this distance is roughly the same as in native concanavalin A.

Some parts of the structure have unusually high temperature factors accompanied by weak density in the map and negative regions in the $(|F_o| - |F_c|) \exp(i\alpha_c)$ map, with no unaccounted peak nearby. We have interpreted such features as disorder. Examples are the side-chain of Glu8 beyond C_γ, which in the native form is liganded to the transition metal, and the external side-chains in the loop of residues 11 to 23.

4. Discussion

This study has been carried out at what is considered to be an intermediate resolution (3·2 Å) and so, before proceeding to a discussion of the results, it is necessary to consider the reliability of an analysis made at this resolution. In fact, it has been shown from a number of structure determinations at about this resolution that it is quite adequate for visualising the polypeptide backbone and most side-chains (Matthews, 1977). Molecular replacements at intermediate resolutions have been used successfully to elucidate conformational differences between similar structures in different crystal forms (Anderson, 1975; Fehlhammer *et al.*, 1975; Moult *et al.*, 1976; Schmid & Herriott, 1976), and the CORELS refinement procedure, when applied to a tRNA at 2·7 Å resolution, proved very effective in clarifying a number of structural details (Sussman *et al.*, 1978).

It is clear that, in the present work too, this refinement procedure has greatly improved the clarity and interpretability of the maps (cf. Figs 2 and 8) to the point where individual side-chains can generally be distinguished. Inspection of the maps provides the best check of the reliability of the interpretation. Comparison of a difference map including an incorrectly positioned length of chain (Fig. 3) with that for the final structure (Fig. 7) indicates that major errors in the model would be immediately apparent. The $(2|F_o| - |F_c|) \exp(i\alpha_c)$ maps (Fig. 8) show that nearly all the atoms are positioned centrally within strong electron density which is well localized so that quite small changes in co-ordinates (~0·5 Å) would worsen this fit. For atoms so situated there can be little doubt of the correctness of the model. For the few regions where electron density and atomic positions are not so well matched the situation is less clear. Portions of the structure in weak density also have high temperature factors and occur on the surface of the molecule or other places where flexibility might reasonably be expected (cf. Results, section (c)). The very few peaks not assigned to atoms are generally much weaker than the rest of the density and outside the protein region (see Fig. 8) as might be expected for solvent or ions. Though we cannot be certain of their interpretation in every case the paucity and sparse distribution of the poorly matched regions in the maps would effectively rule out major misinterpretations in our model, though the possibility of some local errors cannot be excluded.

The presence of two crystallographically independent monomers, which turn out to have closely similar structures, also provides a useful check of our model. We have

(a)

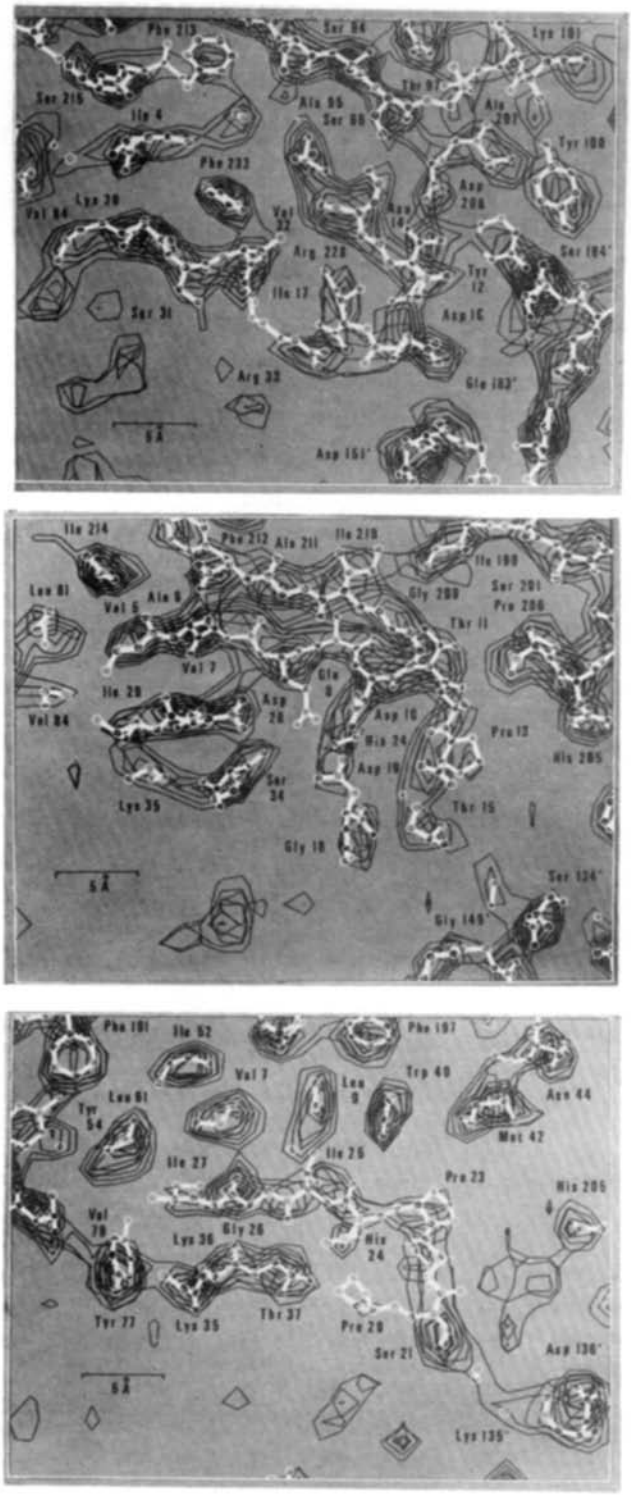

FIG. 8. Three successive 5 Å-thick portions of the electron density map for the refined structure of demetallized concanavalin A in the metal-binding region, sectioned along the z-axis. The coefficients of the Fourier summation are $(2|F_o| - |F_c|) \exp(i\alpha_c)$. Contours are drawn from a level corresponding to the standard deviation (σ) in the non-protein part of the map in equal intervals of half that value. Superimposed is the atomic model. Residue numbers designated with

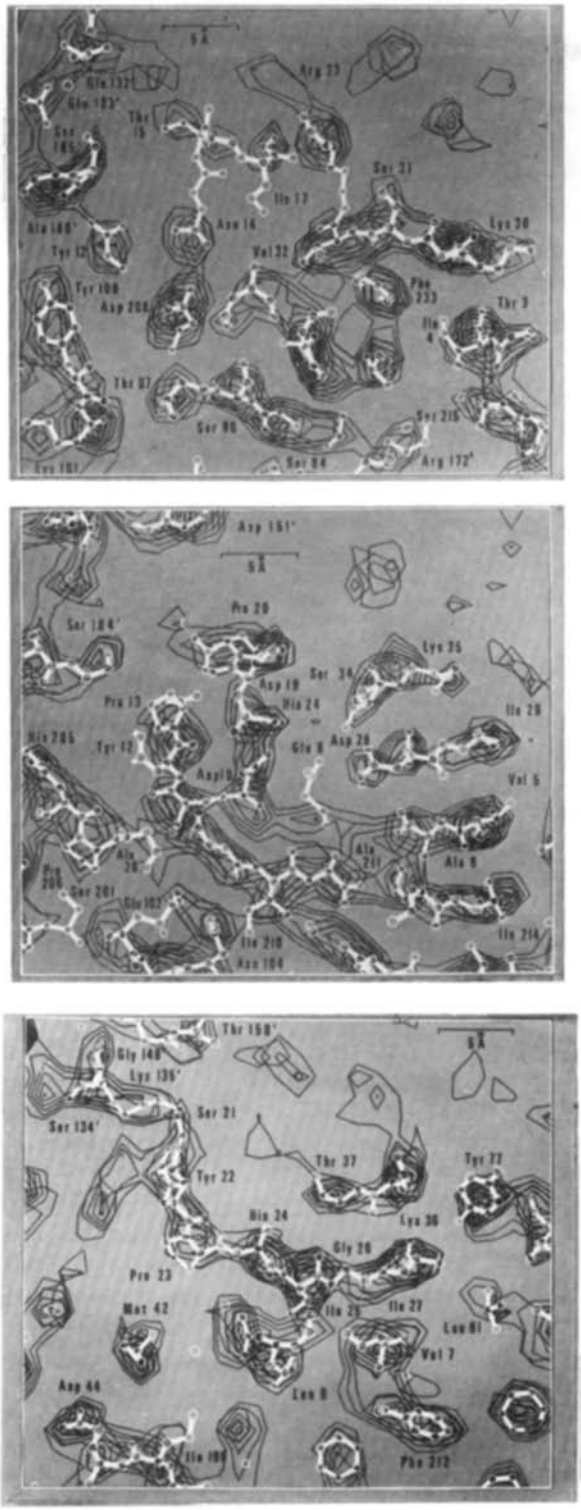

(b)

a superscript are from a neighbouring molecule. (a) Protomer I. (b) Protomer II. Note the high correlation between lack of density here and the corresponding negative density in the difference map shown in Fig. 7. See, for example, Glu8 and Pro20 in Protomer I. We have interpreted such features as representing disorder.

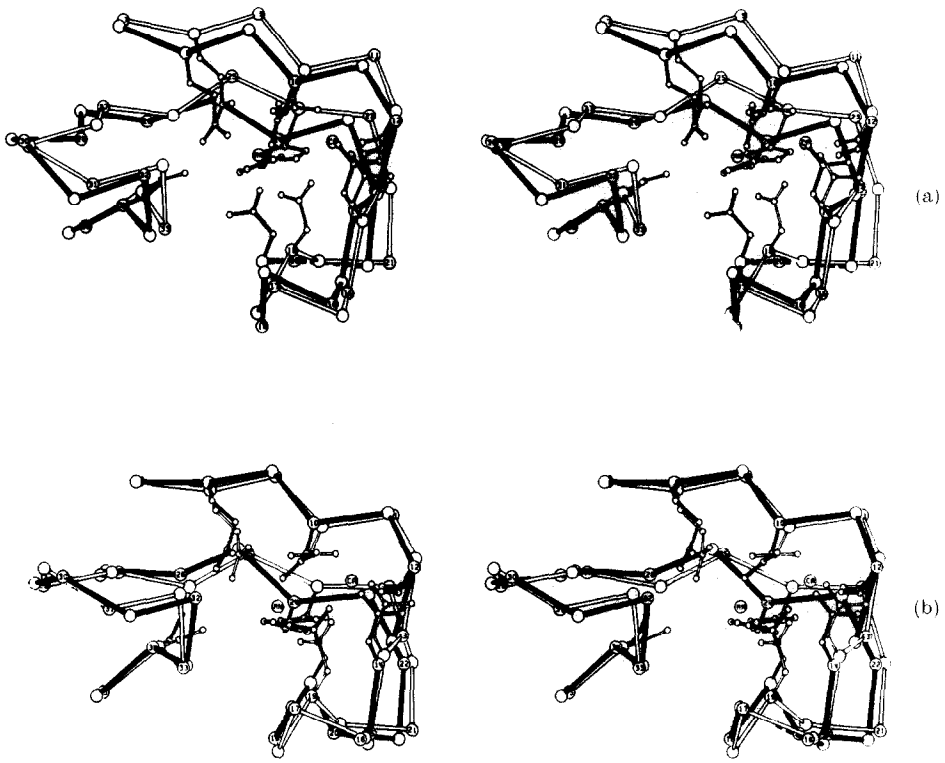

FIG. 9. Stereo representation of residues 7 to 35 in demetallized and native concanavalin A viewed down the *z*-axis. The backbone is represented by virtual bonds between successive alpha-carbons. Details are shown of ligands which participate in metal binding, including the carbonyl group of Tyr12 and side-chains of Glu8, Asp10, Asn14, Asp19, His24 and Ser34. The native structure is the initial starting model used in the refinement process (see text). Flexible parts are shown in dashed lines. (a) Protomer I (solid lines) and native (open lines). (b) Protomer II (solid lines) and native (open lines), rotated by 180° to have roughly the same orientation as protomer I.

tried to estimate the likely error in the co-ordinates by comparing these for equivalent atoms in the monomers excluding those groups which are particularly flexible or might have different conformations because of different intermolecular contacts. The r.m.s. difference in these co-ordinates is 0·6 Å, whereas the r.m.s. co-ordinate shift effected by the refinement is about twice this value (Table 2).

In establishing the differences between the native and demetallized structures we have been hindered by the current unrefined state of the structure of the former. However, several significant comparisons do emerge. The most striking feature of the demetallized structure is the close similarity to the native protein. Main-chain differences are small (2·4 Å at most), there are only a few side-chain rearrangements, and the level of differences for the metal-binding region is similar to that of the rest of the structure. There is some local disorder in the backbone which may explain the greater susceptibility of the demetallized protein to proteolysis (Blumberg & Tal, 1976). Larger differences might have been expected in view of the loss of sugar-binding capacity upon removal of the metals (Yariv *et al.*, 1968), even though the sugar-binding site seems to be about 10 Å from the Mn^{2+}-site (Brewer *et al.*, 1973; Villafranca & Viola, 1974; Alter & Magnuson, 1974). In the following discussion of

differences between the structures we concentrate on one of the two protomers (I) and comment on the differences between protomers at the end.

The Mn^{2+} ligands on the protein (Glu8, Asp10, Asp19 and His24) show the most difference. The side-chain of Glu8 becomes disordered and the distance from the carboxyl group of Asp19 to the imidazole ring of His24 shortens substantially (see Fig. 9). These changes are most easily explained in terms of the changes in charge in the region on removing the metals. For the demetallized structure Glu8, Asp10 and Asp19 may be expected to be negatively charged, and His24 to be positively charged at the pH of crystallization (5·0). Thus, in the demetallized structure, charge–charge interactions stabilize the relationship between Asp10, Asp19 and His24, while Glu8, in the absence of an interaction with the metal or any other stabilizing interaction, becomes disordered. The involvement of Asp19 in a strong interaction is supported by the higher density and lower temperature factor of the side-chain of this residue compared with its backbone (see Fig. 8(a), middle, and 8(b), middle). The presence of a positively charged His24 is also borne out by the report of Gachelin *et al.*, (1972) that two protons are lost on metal-binding. However, we cannot unequivocally account for the second proton.

This rearrangement of residues 10, 19 and 24 suggests an explanation for the metal-free protein's inability to bind calcium. Asp19 is 2 Å further away from the Ca-site than in the native structure (see Figs 9(a) and 10), substantially worsening the liganding situation. However, when a transition metal ion is bound in site S1, His24 loses its positive charge, and the carboxyl groups of Asp10 and Asp19 would presumably be reoriented in accordance with the new charge distribution, creating site S2 for Ca^{2+} binding. This view is supported by the report that calcium can be bound even to the Mn-free protein at pH 7, when the histidine would be uncharged (Alter *et al.*, 1977).

In protomer II these rearrangements are not so pronounced (see Fig. 9(b)). However, there are indications of possible additional backbone disorder (see residues 14 to 17 in Fig. 8(b), top), and there is also a close contact with a neighbouring molecule in the region of residue 16 not present in the other protomer. We therefore believe that the protomer I structure better represents the situation in solution.

It should be noted that our results disagree with those of Becker *et al.* (1976), who report an opening of the loop of residues 11 to 23 in the demetallized structure. We can find no evidence for such a change in our maps after refinement. In a recent paper (Reeke *et al.*, 1978) this group has also reported that the peptide linkage between Ala207 and Asp208, which was assigned a *cis* configuration in native concanavalin A, is *trans* in the demetallized structure, and they have suggested that this might be related to the measurement, from a kinetic analysis of nuclear magnetic resonance data, of a 22 kcal mol^{-1} energy barrier in the activation of the demetallized protein (Brown *et al.*, 1977). However, careful examination of these regions of the structure in both protomers using difference and chopped difference maps have shown us that *cis* configurations fit our electron density maps very well (Fig. 10). The *trans* configurations we have tried to fit to the maps have proved much less satisfactory.

The structural reason for the inability of demetallized concanavalin A to bind saccharides is currently difficult to explain, as the sugar ligands have not been unambiguously identified. However, residues likely to be involved in saccharide binding have been suggested from the location of iodine atoms in iodinated sugar derivatives associated with concanavalin A (Becker *et al.*, 1976; Hardman & Ainsworth, 1976).

FIG. 10. Stereoscopic view of a 12 Å-thick portion of a "chopped" difference electron density map for the refined structure of demetallized concanavalin A in the region of protomer I near residues 20 through 26 as well as His205, Pro206, Ala207, Asp208, Gly209, Ile210 and Ala211. The coefficients of the Fourier summation are $(|F_o| - |F_c|) \exp(i\alpha_c)$ with all residues but 205 through 211 of protomers I and II included in the calculation of structure-factor amplitudes and phases. Contours are drawn at a level corresponding to 2 standard deviations (σ) in the whole map. Superimposed is the refined structural model. Note that there is no appreciable electron density except in the portion of the map corresponding to the 7 residues omitted from the structure-factor calculations and that this fits well with the superimposed structure having a *cis* configuration for the peptide linkage between Ala207 and Asp208 and a *trans* configuration for all the others.

Among these possible saccharide ligands, the positions of the hydroxyls of Tyr12 and Tyr100 deviate by roughly 1·5 Å from their locations in native concanavalin A, and the positions of carboxyl carbon atoms of Asp16 and Asp208 deviate by 1·0 Å and of carbon C_z of Arg228 by 1·5 Å. These differences could perhaps account for the lack of binding capacity for saccharides. A detailed evaluation of the conformational changes in sugar ligands will however have to await the elucidation of the structure of a concanavalin A–saccharide complex.

We thank Drs Mike James, Alberto Podjarny and Paul Sigler for many fruitful discussions, Dr Anita Sielecki for skilful assistance in the computations, Mr Shmuel Gattegno and Mrs Hanna Shkedi for assistance in drawing maps and building molecular models, and the Weizmann Institute Photography Laboratory, for preparing the half-tone electron density map illustrations. We are grateful to Dr Karl D. Hardman for providing us with co-ordinates of native concanavalin A prior to their publication. We would also like to express our appreciation of research grants from the Volkswagen Stiftung (AZ11-1790) and the Minerva Foundation and of a fellowship to one of us (J.M.) from the European Molecular Biology Organization.

REFERENCES

Alter, G. M. & Magnuson, J. A. (1974). *Biochemistry*, **13**, 4038–4045.

Alter, G. M., Pandolfino, E. R., Christie, D. J. & Magnuson, J. A. (1977). *Biochemistry*, **16**, 4034–4038.

Anderson, L. (1975). *J. Mol. Biol.* **94**, 33–49.

Barber, B. H. & Carver, J. P. (1973). *J. Biol. Chem.* **248**, 3353–3355.

Becker, J. W., Reeke, G. N. Jr, Wang, J. L., Cunningham, B. A. & Edelman, G. M. (1975). *J. Biol. Chem.* **250**, 1513–1524.

Becker, J. W., Reeke, G. N. Jr, Cunningham, B. A. & Edelman, G. M. (1976). *Nature (London)*, **259**, 406–409.

Blumberg, S. & Tal, N. (1976). *Biochim. Biophys. Acta*, **453**, 357–364.

Brewer, C. F., Sternlicht, H., Marcus, D. M. & Grollman, A. P. (1973). *Proc. Nat. Acad. Sci., U.S.A.* **70**, 1007–1011.

Brown, R. D., Brewer, C. F. & Koenig, S. H. (1977). *Biochemistry*, **16**, 3883–3896.

Diamond, R. (1974). *J. Mol. Biol.* **82**, 371–391.

Edelman, G. M., Cunningham, B. A., Reeke, G. N. Jr, Becker, J. W., Waxdal, M. J. & Wang, J. L. (1972). *Proc. Nat. Acad. Sci., U.S.A.* **69**, 2580–2584.

Fehlhammer, H., Schiffer, M., Epp, O., Colman, P. M., Lattman, E. E., Schwager, P., Steigemann, W. & Schramm, H. J. (1975). *Biophys. Struct. Mechanism*, **1**, 139–146.

Gachelin, G., Goldstein, L., Hofnung, D. & Kalb, A. J. (1972). *Eur. J. Biochem.* **30**, 155–162.

Goldammer, E. von & Zorn, H. (1974). *Eur. J. Biochem.* **44**, 195–199.

Hardman, K. D. & Ainsworth, C. F. (1972). *Biochemistry*, **11**, 4910–4919.

Hardman, K. D. & Ainsworth, C. F. (1975). *The Protein Data Bank*. Brookhaven National Laboratory, Upton, New York.

Hardman, K. D. & Ainsworth, C. F. (1976). *Biochemistry*, **15**, 1120–1128.

Hardman, K. D., Wood, M. K., Schiffer, M., Edmundson, A. B. & Ainsworth, C. F. (1971). *Proc. Nat. Acad. Sci., U.S.A.* **68**, 1393–1397.

Jack, A., Weinzierl, J. & Kalb, A. J. (1971). *J. Mol. Biol.* **58**, 389–395.

Kalb, A. J. & Levitzki, A. (1968). *Biochem. J.* **109**, 669–672.

Kalb, A. J. & Pecht, I. (1973). *Biochim. Biophys. Acta*, **303**, 264–268.

Luzzati, V. (1953). *Acta Crystallogr.* **6**, 142–152.

Matthews, B. W. (1977). In *The Proteins* (3rd edition) (Neurath H. & Hill, R. L., eds), vol. 3, pp. 445–446, Academic Press, New York.

Meirovitch, E. & Kalb, A. J. (1973). *Biochim. Biophys. Acta*, **303**, 258–263.

Meirovitch, E., Luz, Z. & Kalb (Gilboa), A. J. (1974). *J. Amer. Chem. Soc.* **96**, 7542–7546.

Moult, J., Yonath, A., Traub, W., Smilansky, A., Podjarny, A., Rabinovich, D. & Saya, A. (1976). *J. Mol. Biol.* **100**, 179–195.

Nicolau, C., Kalb, A. J. & Yariv, J. (1969). *Biochim. Biophys. Acta*, **194**, 71–73.

North, A. C. T., Phillips, D. C. & Mathews, F. S. (1968). *Acta Crystallogr. sect. A*, **24**, 351-359.

Nyburg, S. C. (1974). *Acta Crystallogr. sect. B*, **30**, 251–253.

Quiocho, F. A., Reeke, G. N. Jr, Becker, J. W., Lipscomb, W. N. & Edelman, G. M. (1971). *Proc. Nat. Acad. Sci., U.S.A.* **68**, 1853–1857.

Reeke, G. N. Jr, Becker, J. W. & Edelman, G. M. (1975). *J. Biol. Chem.* **250**, 1525–1547.

Reeke, G. N. Jr, Becker, J. W. & Edelman, G. M. (1978). *Proc. Nat. Acad. Sci., U.S.A.* **75**, 2286–2290.

Rollett, J. S. & Sparks, R. A. (1960). *Acta Crystallogr.* **13**, 273–274.

Rossmann, M. G. (1972). In *The Molecular Replacement Method*, International Science Review Series, vol. 13, Gordon and Breach, New York.

Schmid, M. F. & Herriott, J. R. (1976). *J. Mol. Biol.* **103**, 175–190.

Shoham, M., Kalb, A. J. & Pecht, I. (1973). *Biochemistry*, **12**, 1914–1917.

Shoham, M., Sussman, J. L., Yonath, A., Moult, J., Traub, W. & Kalb (Gilboa), A. J. (1978). *FEBS Letters*, **95**, 54–56.

Sumner, J. B. (1919). *J. Biol. Chem.* **37**, 137–142.

Sumner, J. B. & Howell, S. F. (1936). *J. Biol. Chem.* **115**, 583–588.

Sussman, J. L., Holbrook, S. R., Church, G. M. & Kim, S. H. (1977). *Acta Crystallogr. sect. A*, **33**, 800–804.

Sussman, J. L., Holbrook, S. R., Warrant, R. W., Church, G. M. & Kim, S. H. (1978). *J. Mol. Biol.* **123**, 607–630.

Villafranca, J. J. & Viola, R. E. (1974). *Arch. Biochem. Biophys.* **160**, 465–468.

Watenpaugh, K. D., Sieker, L. C., Herriott, J. R. & Jensen, L. H. (1973). *Acta Crystallogr. sect. B*, **29**, 943–956.

Watson, H. C., Shotton, D. M., Cox, J. M. & Muirhead, H. (1970). *Nature (London)*, **225**, 806–811.

Weinzierl, J. & Kalb, A. J. (1971). *FEBS Letters*, **18**, 268–270.

Yariv, J., Kalb, A. J. & Levitzki, A. (1968). *Biochim. Biophys. Acta*, **165**, 303–305.